Tuning transfer function of fiber-optic Fabry–Pérot interferometer via introduction of birefringence in the cavity

Marzena HIRSCH*, Paweł WIERZBA, Małgorzata JĘDRZEJEWSKA-SZCZERSKA

Department of Metrology and Optoelectronics,
Faculty of Electronics, Telecommunications and Informatics,
Gdańsk University of Technology, Narutowicza 11/12, 80-233 Gdańsk, Poland

*Corresponding author: hirsch.marzena@gmail.com

The study investigates the impact of birefringence exhibited by the cavity material of a fiber-optic Fabry–Pérot interferometer on its transfer function. The theoretical approach to analyze the effect of birefringence in the cavity of a plane Fabry–Pérot interferometer is described. The case of high- and low-finesse interferometer is investigated. It is shown that introduction of a birefringent medium of optimized parameters can be used to increase the density of interference fringes in certain wavelength range – the feature can be used either for reduction of the cavity length in an interferometric sensor or operation with sources of narrower spectral characteristics.

Keywords: fiber-optic interferometer, birefringence, fiber optic sensors, Fabry–Pérot interferometer.

1. Introduction

For the last few decades the design of fiber-optic interferometric sensors has been the field of extensive research in a broad range of applications [1–3]. The Fabry–Pérot sensing interferometers are widely employed in industry and research laboratories – due to their metrological performance, as well as their simplicity and versatility. Such interferometric sensors offer high precision of measurements while using low-power light sources. It allows for safe operation in hazardous environment and for measurements of fragile biochemical samples. Small size of the fiber-optic Fabry–Pérot sensing interferometers (often about tens of micrometers) reduces the volume of a sample needed for measurement to nanoliters. It makes them a promising candidate for biomedical, chemical and biophotonic applications. Some of the successful applications that have been demonstrated thus far include measurements of volatile organic compounds [4], hematocrite level [5], refractive index sensing of liquids and gases [6–8] as well as temperature and pressure sensors [9–12].

The subsequent discussion covers low-coherence Fabry–Pérot sensors. The particular advantage of these sensors is that the results are immune from fluctuation in the power level of the optical radiation that reaches the detection setup, as the relevant data is encoded in spectral domain of the optical signal. In a commonly used setup, the sensing interferometer is illuminated by a broadband light source – like a super luminescent diode (SLD) or an amplified spontaneous emission (ASE) source. The detection setup consists of a spectral processing device – a spectrometer or an optical spectrum analyser (OSA).

The media present in the cavity of a sensing fiber-optic Fabry–Pérot interferometer are almost invariably isotropic. However, operation of such an interferometer in the presence of birefringence in the cavity is also worthwhile to consider as it can be used to adjust the metrological parameters of the device for specific applications. Our investigation is aimed at evaluation and tuning of the metrological parameters of a fiber-optic sensor based on a Fabry–Pérot interferometer when its cavity is filled by a uniaxial birefringent medium with optical axis parallel to reflective surfaces of the interferometer.

2. Theory

An optical fiber Fabry–Pérot interferometer is formed by two flat surfaces S_1 and S_2 of an optical fiber separated by a distance h, as shown in Fig. 1. Reflections from surfaces S_1 and S_2 arise either due to Fresnel reflections or as a result of a reflective layer applied on S_1 or S_2.

In the former case, the reflectivity R at each surface is given by [13]:

$$R = \left(\frac{n_1 - n_2}{n_1 + n_2} \right)^2 \tag{1}$$

where n_1 is the refractive index of the fiber, and n_2 – the refractive index of the medium in the cavity.

The investigation is focusing on the case of Fabry–Pérot interferometers operated in the reflective configuration, as it is the most widely used in fiber-optic sensors. The analysis is conducted with assumption of the plane wave propagation in the interferometer in order to elicit key features of the reflected signal most clearly.
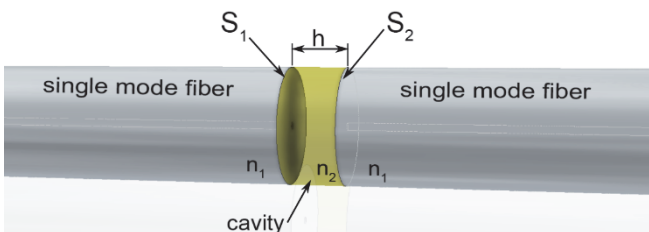

Fig. 1. Optical fiber Fabry–Pérot interferometer: h – length of the cavity, n_1 – refractive index of the fiber core, and n_2 – refractive index of the medium in the cavity.

First, let us consider a plane Fabry–Pérot interferometer with an isotropic medium in its cavity, illuminated by a plane wave of intensity I_i. Let us also assume that the wave is either unpolarised or circularly polarized. For normal incidence, phase δ corresponding to the round trip of radiation in the cavity is given by

$$\delta = 2\pi \frac{2n_2 h}{\lambda_0} \tag{2}$$

where h is the cavity length, λ_0 – wavelength, n_2 – refractive index of the medium in the cavity.

The intensity of the plane wave I_r reflected by this interferometer is given by [13]:

$$I_r = \frac{F\sin^2(\delta/2)}{1 + F\sin^2(\delta/2)} I_i \tag{3}$$

where δ is the phase difference introduced in the cavity, and F – finesse factor of value defined as

$$F = \frac{4\sqrt{R_1 R_2}}{\left(1 - \sqrt{R_1 R_2}\right)^2} \tag{4}$$

where $R_{1,2}$ denotes the reflectivity of the cavity surfaces.

However, if the cavity of the Fabry–Pérot interferometer is filled with a uniaxial birefringent medium whose optical axis is parallel to reflective surfaces S_1 and S_2, the propagation of light in the interferometer changes. On entering the cavity, the plane wave is divided into two waves – one polarized along the optical axis and the other polarized perpendicularly to the optical axis. The waves are known as ordinary and extraordinary. Their phase velocities are:

$$v_o = c/n_o \tag{5a}$$

$$v_e = c/n_e \tag{5b}$$

respectively, for ordinary and extraordinary beam, where c – velocity of light in vacuum, n_o – ordinary refractive index of the medium, n_e – extraordinary refractive index of the medium.

The amplitudes A_o and A_e of these waves depend on the state of polarization of the incident wave, and the sum of the intensities of ordinary (I_o) and extraordinary (I_e) waves can be written as [14]:

$$|A_o|^2 + |A_e|^2 = I_o + I_e = I_i \tag{6}$$

where I_i is the intensity of the plane wave entering the cavity.

When the direction of the optical axis is constant in the material and no significant scattering takes place, ordinary and extraordinary waves propagate without exchang-

ing energy. Therefore, they can be considered separately. For each of these waves formulas (2)–(4) are valid, with n_o or n_e replacing n_2. In particular, the total intensity of the plane wave reflected by this interferometer, given by (3), can be expressed as a sum of the ordinary ($I_{r,o}$) and extraordinary ($I_{r,e}$) component:

$$I_r = I_{r,o} + I_{r,e} = \frac{F\sin^2(\delta_o/2)}{1 + F\sin^2(\delta_o/2)}\alpha I_i + \frac{F\sin^2(\delta_e/2)}{1 + F\sin^2(\delta_e/2)}\beta I_i \qquad (7)$$

where F is given by (4), δ_o, δ_e are calculated as in (2) by replacing n_2 with n_o and n_e, respectively, and α, β are the coefficients corresponding to the amplitudes of the ordinary and extraordinary waves ($\alpha, \beta \in [0, 1]$).

When the incident wave is either unpolarised or is circularly polarized, α and β vary much faster than the measurement time of the intensity. As a result, the detector reacts to their average value as close to 0.5 ($\alpha \approx 0.5$, $\beta \approx 0.5$) and (7) becomes

$$I_r \approx \frac{F\sin^2(\delta_o/2)}{1 + F\sin^2(\delta_o/2)}\frac{I_i}{2} + \frac{F\sin^2(\delta_e/2)}{1 + F\sin^2(\delta_e/2)}\frac{I_i}{2} \qquad (8)$$

3. Results and discussion

When reflectivity of the mirrors is high ($F \gg 1$), the contrast of interference fringes is high. Then, reflection spectra ($I_r(\lambda)/I_i(\lambda)$) become the superposition of two sets of interference fringes, formed by the ordinary and extraordinary wave. The fringe patterns are completely or partially overlapping, the shift between them is dependent on the phase difference $\delta_e - \delta_o$. Example spectra, calculated for the phase shift equal to π and $\pi/5$, are presented in Fig. 2.

Shape of the output spectra, presented in Figs. 2**c** and 2**d** is strongly influenced by the value of phase difference $\delta_e - \delta_o$. When $\delta_e - \delta_o = \pi$ (or its odd multiple), the number of fringes increases twice, comparing to the spectrum of an interferometer with isotropic medium in the cavity. If $\delta_e - \delta_o$ is close to 2π (or its multiple), the ordinary and extraordinary component are in sync and the resultant spectrum is the same as in the case of isotropic cavity. In the case where value of $\delta_e - \delta_o$ is in-between those values, the output interference pattern also contains two sets of fringes but of unequal amplitude and width – as is shown for $\delta_e - \delta_o = \pi/5$ in Fig. 2**d**.

What should also be noted is that while the overlapping of the I_o and I_e fringes gives denser interference pattern, it also results in the decrease of the contrast ratio. Usually, high contrast of the fringes is desired in the analysis of interferometric measurements. However, many signal processing techniques commonly used in these types of sensors require at least a few fringes to be recorded. The density of the fringe pattern is dependent on the refractive index of the cavity medium as well as on its geometrical length. An increase of the number of fringes can be used in interferometers with short cavity to reduce the spectral range in which the measurement has to be performed. The reduction
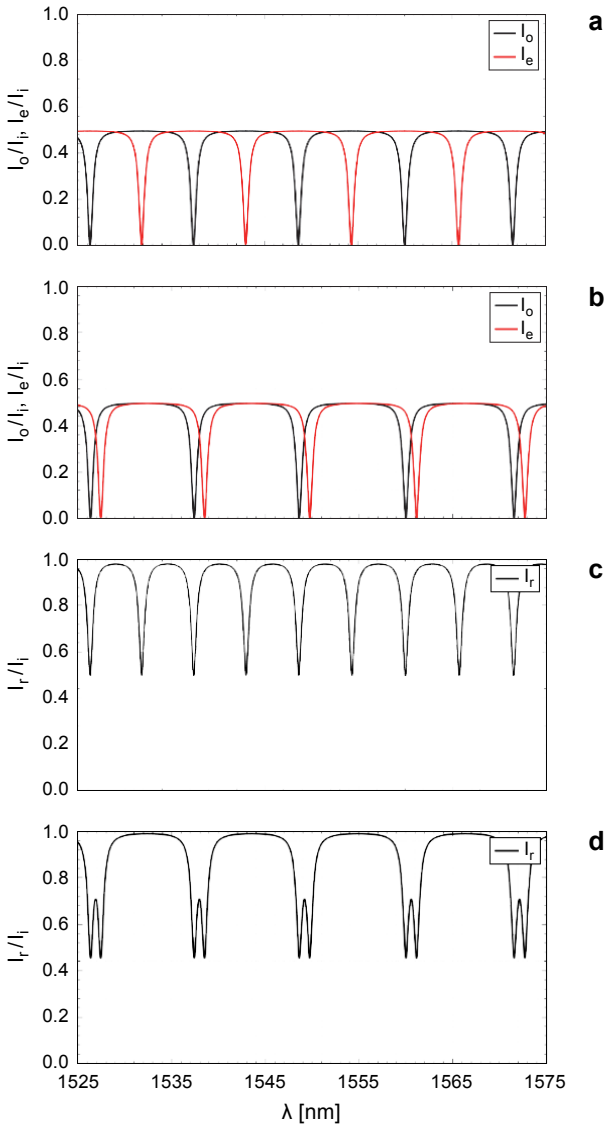
Fig. 2. Fabry–Pérot interferometer with high F value ($F = 100$): ordinary (I_o) and extraordinary (I_e) components of reflection spectra, when $\delta_e - \delta_o = \pi$ (**a**) and when $\delta_e - \delta_o = \pi/5$ (**b**), and the reflection spectra, when $\delta_e - \delta_o = \pi$ (**c**) and when $\delta_e - \delta_o = \pi/5$ (**d**).

of the required wavelength range can be beneficial for the sensor setup as it allows for operation with light sources with narrower spectral characteristic – those usually come at a lower cost and are more easily available. Another field of application where shorter cavity is a potential advantage are measurements of samples of very small volume (*e.g.* in biomedical applications) or samples of strongly absorbing substances.

In practical applications one needs to take into account that the phase shift of ordinary and extraordinary waves is dependent on the wavelength. Therefore, to achieve doubling of the fringes in the desired wavelength range, parameters ($n_o - n_e$, h) of the birefringent cavity must be set to suitable values. In Fig. 3 a comparison is presented of the spectra simulated for cavity with $n_o - n_e$ value equal 0.04 but with two different lengths (68 and
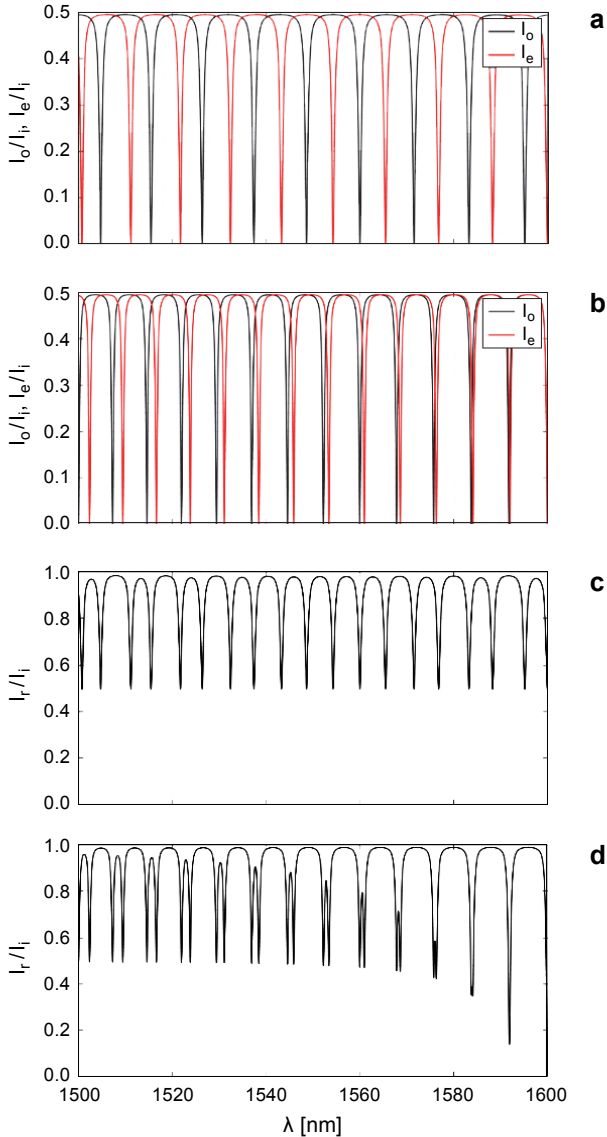

Fig. 3. Fabry–Pérot interferometer with high F value ($F_e = 100$): I_o and I_e components (**a**) and the reflection spectra (**c**), when $n_o = 1.56$, $n_e = 1.6$, $h = 68$ μm; I_o and I_e components (**b**) and the reflection spectra (**d**), when $n_o = 1.56$, $n_e = 1.6$, $h = 100$ μm.

100 μm). The example of 68 μm cavity (Figs. 3**a** and 3**c**) shows that it is possible to achieve the coverage of doubled fringes over the 60 nm wavelength range (from 1520 to 1580 nm in Fig. 3**c**). It is sufficient for most applications as the spectral characteristics of the light sources usually employed in low-coherence interferometry exhibit the full-width at half-maximum ($\Delta\lambda_{FWHM}$) below 100 nm. In case of the 100 μm cavity (Figs. 3**b** and 3**d**) in the same wavelength range, the value of phase difference $\delta_e - \delta_o$ is changed, varying closer to the increment of 2π than in the previous case. In Fig. 3**d** it can be observed that the visibility of one set of the fringes is gradually reduced as the wavelength is increasing. At 1600 nm the ordinary and extraordinary fringes are almost in sync (Fig. 3**c**), resulting in the spectra similar as for isotropic cavity. Setting the parameters to achieve that result can also be useful in some cases – if the birefringence of the investigated medium in the cavity is a nuisance, its effect can be compensated by adjusting the cavity length.

The representative spectra shown in Fig. 3 are calculated for a high finesse interferometer. In conventional fiber optic Fabry–Pérot interferometers (with glass-cavity Fresnel reflections) the reflectivity of the cavity boundaries, and thus the interferometer finesse, is usually lower. However, a finesse of the interferometer setup can be increased to achieve satisfactory contrast of the interference pattern. The development in nanotechnology and techniques of depositing thin films opened new opportunities for fine tuning the finesse of conventional fiber-optic Fabry–Pérot interferometers. In order to modify the reflectance of S_1 or S_2 (Fig. 1), an additional reflective layer can be deposited on these surfaces. Thin (tens of nanometers) dielectric films made from materials with high refractive index (*e.g.* ZnO, TiO_2 [15, 16]) or low refractive index (such as a nanolattice material [17]) can be used to modify the reflectance of the fiber-cavity interface. The thin, semi-transparent metal films made from, *e.g.* silver, aluminium or gold can be applied as well. In the case of the Fabry–Pérot interferometer operated in reflection mode, a thick high-reflectivity metal or dielectric mirror can be used as S_2 surface.

4. Conclusion

In conclusion, we presented an insight into a possible beneficial application of birefringence introduced in the Fabry–Pérot cavity. The theoretical discussion analysed what impact on the performance can be expected in case of various parameters of the birefringent material. Possibility to achieve doubling of the interference fringes in certain wavelength range can be a useful feature that allows for reduction of the cavity length (and thus sample volume), while maintaining similar interference pattern resolution, or reducing the bandwidth of the source used in the sensor.

References

[1] Md. Rajibul Islam, Muhammad Mahmood Ali, Man-Hong Lai, Kok-Sing Lim, Harith Ahmad, *Chronology of Fabry–Perot interferometer fiber-optic sensors and their applications: a review*, Sensors **14**(4), 2014, pp. 7451–1788, DOI: 10.3390/s140407451.

[2] Yi Wen Huang, Jin Tao, Xu Guang Huang, *Research progress on F-P interference—based fiber-optic sensors*, Sensors **16**(9), 2016, article ID 1424, DOI: 10.3390/s16091424.

[3] Ascorbe J., Corres J.M., Arregui F.J., Matias I.R., *Recent developments in fiber optics humidity sensors*, Sensors **17**(4), 2017, article ID 893, DOI: 10.3390/s17040893.

[4] Cai-Bin Yu, Yu Wu, Chen Li, Fan Wu, Jin-Hao Zhou, Yuan Gong, Yun-Jiang Rao, Yuan-Fu Chen, *Highly sensitive and selective fiber-optic Fabry–Perot volatile organic compounds sensor based on a PMMA film*, Optical Materials Express **7**(6), 2017, pp. 2111–2116, DOI: 10.1364/OME.7.002111.

[5] Jędrzejewska-Szczerska M., *Response of a new low-coherence Fabry–Perot sensor to hematocrit levels in human blood*, Sensors **14**(4), 2014, pp. 6965–6976, DOI: 10.3390/s140406965.

[6] Ben Xu, Yi Yang, Zhenbao Jia, Wang D.N., *Hybrid Fabry–Perot interferometer for simultaneous liquid refractive index and temperature measurement*, Optics Express **25**(13), 2017, pp. 14483–14493, DOI: 10.1364/OE.25.014483.

[7] Cheng-Ling Lee, Hsuan-Yu Ho, Jheng-Hong Gu, Tung-Yuan Yeh, Chung-Hao Tseng, *Dual hollow core fiber-based Fabry–Perot interferometer for measuring the thermo-optic coefficients of liquids*, Optics Letters **40**(4), 2015, pp. 459–462, DOI: 10.1364/OL.40.000459.

[8] Pinggang Jia, Guocheng Fang, Ting Liang, Yingping Hong, Qiulin Tan, Xiaoyong Chen, Wenyi Liu, Chenyang Xue, Jun Liu, Wendong Zhang, Jijun Xiong, *Temperature-compensated fiber-optic Fabry–Perot interferometric gas refractive-index sensor based on hollow silica tube for high-temperature application*, Sensors and Actuators B: Chemical **244**, 2017, pp. 226–232, DOI: 10.1016/j.snb.2016.12.123.

[9] Guigen Liu, Qiwen Sheng, Weilin Hou, Ming Han, *High-resolution, large dynamic range fiber-optic thermometer with cascaded Fabry–Perot cavities*, Optics Letters **41**(21), 2016, pp. 5134–5137, DOI: 10.1364/OL.41.005134.

[10] Poeggel S., Duraibabu D., Kalli K., Leen G., Dooly G., Lewis E., Kelly J., Munroe M., *Recent improvement of medical optical fibre pressure and temperature sensors*, Biosensors **5**(3), 2015, pp. 432–449, DOI: 10.3390/bios5030432.

[11] Ben Xu, Chao Wang, Wang D.N., Yaming Liu, Yi Li, *Fiber-tip gas pressure sensor based on dual capillaries*, Optics Express **23**(18), 2015, pp. 23484–23492, DOI: 10.1364/OE.23.023484.

[12] Jiajun Tian, Yuzhu Jiao, Shaobo Ji, Xiaolong Dong, Yong Yao, *Cascaded-cavity Fabry–Perot interferometer for simultaneous measurement of temperature and strain with cross-sensitivity compensation*, Optics Communications **412**, 2018, pp. 121–126, DOI: 10.1016/j.optcom.2017.12.005.

[13] Born M., Wolf E., *Principles of Optics: Electromagnetic Theory of Propagation, Interference and Diffraction of Light*, 7th (expanded) Ed., Cambridge University Press, Cambridge, 1999.

[14] Saleh B.E.A., Teich M.C., *Fundamentals of Photonics*, 2nd Ed., Hoboken, N.J., Wiley Interscience, 2007.

[15] Hirsch M., Majchrowicz D., Wierzba P., Weber M., Bechelany M., Jędrzejewska-Szczerska M., *Low-coherence interferometric fiber-optic sensors with potential applications as biosensors*, Sensors **17**(2), 2017, article ID 261, DOI: 10.3390/s17020261.

[16] Majchrowicz D., Hirsch M., Wierzba P., Bechelany M., Viter R., Jędrzejewska-Szczerska M., *Application of thin ZnO ALD layers in fiber-optic Fabry–Pérot sensing interferometers*, Sensors **16**(3), 2016, article ID 416, DOI: 10.3390/s16030416.

[17] Xu A. Zhang, Yi-An Chen, Abhijeet Bagal, Chih-Hao Chang, *Enhanced total internal reflection using low-index nanolattice materials*, Optics Letters **42**(20), 2017, pp. 4123–4126, DOI: 10.1364/OL.42.004123.